Displacive phase-field crystal model

Eli Alster,[1,2] K. R. Elder,[3] and Peter W. Voorhees[2,*]
[1]Department of Chemical and Biological Engineering, Northwestern University, Evanston, Illinois 60208, USA
[2]Department of Materials Science and Engineering, Northwestern University, Evanston, Illinois 60208, USA
[3]Department of Physics, Oakland University, Rochester, Michigan 48309, USA

(Received 29 September 2019; published 21 January 2020)

A phase-field crystal model that spontaneously undergoes displacive phase transitions is introduced by explicitly studying a two-component two-dimensional square crystal reminiscent of a perovskite. When the intercomponent free energy is a simple polynomial, the crystal undergoes displacive transitions in the ⟨10⟩ and ⟨11⟩ directions. When the interaction is a correlation function, displacements in any direction can occur. This displacive phase-field crystal (DPFC) model maps to Landau-Ginzburg-Devonshire (LGD) theories for ferroelectrics, and the DPFC and LGD models are compared in terms of phase transitions and domain walls. Dynamical simulations of quadrijunctions were also performed and found stable spiraling quadrijunctions and unstable nonspiraling quadrijunctions. Last, domain coarsening across a small-angle grain boundary demonstrates multiple forms of non-mean-curvature-driven growth.

DOI: 10.1103/PhysRevMaterials.4.013802

I. INTRODUCTION

A fundamental problem limiting the utility of molecular simulations is the problem of rare events. Namely, current computational technology limits the timescale of ordinary molecular dynamics (MD) simulations to the order of nanoseconds, which is too short to capture phenomena of interest such as protein aggregation [1] and grain motion [2]. Typical long-timescale methods, such as coarse-grained molecular dynamics [3] and phase-field models [4], do not model with atomic resolution. Other models retain atomistic detail but require significant amounts of *a priori* information, such as a transition catalog for kinetic Monte Carlo (KMC) [5] and correct choices of collective variables for accelerated MD [6,7].

Due to these difficulties, the phase-field crystal (PFC) model has gained attention [8]. The PFC model retains atomistic detail, is capable of long-timescale simulations, and does not require *a priori* knowledge about the process one is attempting to simulate. However, unlike MD and KMC, it is a free-energy-functional-based method. Meaning, unlike in MD and KMC, whose potentials are functions of discrete atomic coordinates, in PFC models, the free energy is a function of smooth order parameters, which are interpreted as values averaged over the timescale of atomic vibrations. As a consequence of being a functional method, the extensive work developing accurate potentials for molecular dynamics [9] are not useful, and entirely new potentials must be developed for every new material of interest. Despite some effort to connect the PFC potentials to data from classical density-functional theory [10–12], this approach has unfortunately only been demonstrated to work for body-centered cubic materials. In practice, most PFC models are "empirical" in nature and are fit to assorted data [13–16].

One important empirical model is the structural PFC (XPFC) model [17,18]. In this model, the free energy is

$$F[n] = \int_V \left[\frac{1}{2}n^2 - \frac{1}{6}n^3 + \frac{1}{12}n^4 - \frac{1}{2}nC * n\right]d\boldsymbol{r}, \quad (1)$$

where F is the nondimensionalized free energy, n is the nondimensionalized atomic density, V is the system volume, C is an isotropic two-point correlation function, and $C * n \equiv \int_{V'} C(|\boldsymbol{r} - \boldsymbol{r}'|)n(\boldsymbol{r}')d\boldsymbol{r}'$. Drawing inspiration from classical density-functional theory, the correlation function term is called the "excess" free energy and the polynomial of n the "ideal" energy [19]. The XPFC model's successes are based on the insight that putting peaks in the Fourier transform of the two-point correlation function, $\hat{C}(q)$, at $q = |\boldsymbol{q}|$ values where there are peaks in the materials diffraction pattern stabilizes many structures. Purely motivated by simplicity, the correlation function itself is defined as a sum or supremum of Gaussians so that the q values where extrema occur can be easily specified. As an added benefit, the elastic constants can be controlled by specifying by the second derivative of $\hat{C}$ at those extrema [17,18]. This approach is successful in stabilizing fcc [18], hcp [20], and diamond [21], despite the lack of connection between the correlation functions used in these models and the correlation functions of real liquid-state metals [22]. The connection between the Fourier transform of the target crystal structure, the crystal's structure factor, and $\hat{C}$ was further explored in later work [23,24].

The XPFC model as originally conceived dealt only with single-component crystals. As the vast majority of crystalline materials are multicomponent, there have been a number of extensions. The first extension dealt with substitutional and interstitial alloys. In this case, instead of the free energy being a function of the normalized atomic density of a single component, $F[n_A]$, the free energy is a function of the

*p-voorhees@northwestern.edu

total normalized density and a long-wavelength concentration order parameter, $F[n, c]$ [19,25,26]. In contrast to substitutional alloys, in intermetallic alloys the "concentration" order parameter varies on the length scale of the unit cell, and the long-wavelength approximation is invalid. Instead, intermetallic PFC models utilize an additional correlation function to cause the "concentration" order parameter to vary on the length scale of the unit cell [23,27]. When the intermetallics have exact stoichiometries that do not readily permit substitutions though, models are typically constructed as explicit functions of the separate component densities, $F[n_A, n_B]$, instead [16,24].

Perovskites, which are of interest for applications ranging from solar cells [28,29] to light-emitting diodes [30], are examples of these intermetallics with exact stoichiometries. Motivated by a desire to predict perovskite microstructure, two of the authors recently introduced a simple PFC model that stabilizes the basic perovskite crystal structure [24]. However, a major issue with this model is that it does not exhibit ferroelectricity. At high temperatures, perovskites such as $PbTiO_3$ have a centrosymmetric crystal structure, and on a decrease in temperature, they undergo displacive phase transitions to noncentrosymmetric states [31]. The noncentrosymmetric crystal structures are the source of polarization densities, and the ability of the materials to transform between the multiple symmetry equivalent noncentrosymmetric states on application of an external electric field is the source of the ferroelectricity. The previously developed perovskite model, like other prior multicomponent PFC models, only stabilizes the centrosymmetric state [16,19,23–25,27], making polarization and ferroelectric phenomena impossible.

Although no PFC model exists that demonstrates a displacive phase transition, there does exist a plethora of phase-field models for modeling ferroelectrics. These models, also known as Landau-Ginzburg-Devonshire (LGD) models, postulate a free energy as a function of a polarization vector, gradients in the polarization vector, and elastic strain [32]. This theory has been used to predict topological phase transitions in ferroelectric nanoparticles [33], understand ferroelectric switching and domain wall profiles in perovskites [34–36], and much more [37]. As PFC models naturally incorporate elasticity without requiring an explicit elastic field, Seymour *et al.*, based on similar work in magnetic systems by Faghihi *et al.* [38,39], introduced a model [40] where the free energy is not only a function of the normalized atomic density as usual but also an explicit function of the polarization vector and its gradient. This was accomplished by adding the polarization terms of LGD models to a normal PFC functional [Eq. (1)] and then introducing appropriate coupling terms between the polarization and PFC terms in order to recover the traditional LGD models in the phase-field limit. As might be apparent from the descriptions alone, both Seymour's model and LGD models are quite complex.

In the present work, we introduce a phase-field crystal model for displacive phase transitions that reproduces many of the complex free energies and behaviors of LGD models, without any explicit polarization field. Instead, the polarization is an emergent property. Section II introduces the displacive phase-field crystal (DPFC) model in general and then illustrates it by considering a simple square crystal (Fig. 1).

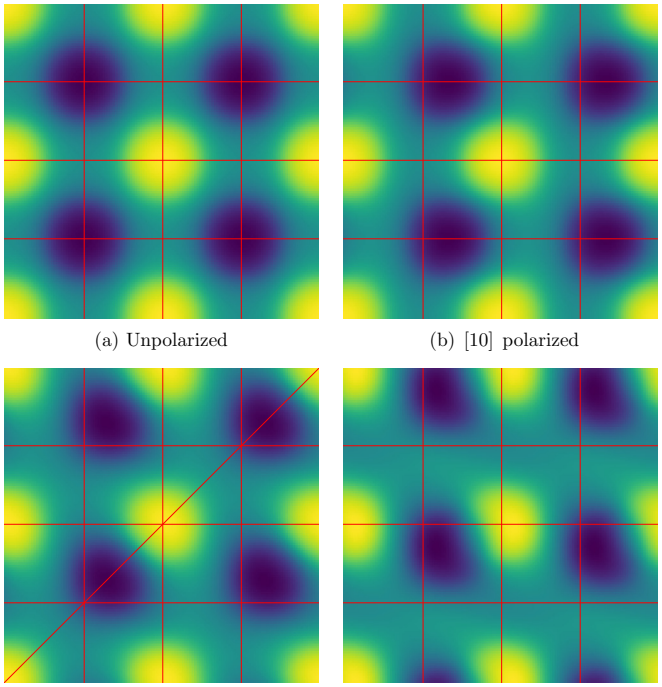

(a) Unpolarized (b) [10] polarized (c) [11] polarized (d) Non-symmetric polarization

FIG. 1. Plots of the unpolarized and polarized states in the two-component square crystal model. The yellow regions (corners and center) are sites for component A, and the dark-blue regions are sites for component B. The red lines are visual aids to show symmetries of the unit cell. Notice that in (d), the site of the dark-blue region possesses no special symmetries.

Using a few simple polynomial interaction terms between the components, displacive transitions in the ⟨10⟩ and ⟨11⟩ directions are shown to be possible, and by using a correlation function for the intercomponent interaction, positioning an atom at any position in the unit cell is demonstrated to be possible as well. Section III compares the DPFC model to LGD theory. Last, Sec. IV verifies that the ⟨10⟩ displacive transition is second order, examines the behavior of domain walls and quadrijunctions, and makes predictions about the interaction of domain walls with grain boundaries.

II. MODEL FORMULATION

In general, the free energy of a two-component system can be decomposed into the free energies of the individual components, F_i, plus an interaction correction, F_{AB}. Namely,

$$F[n_A, n_B] = F_A[n_A] + F_B[n_B] + F_{AB}[n_A, n_B], \tag{2}$$

where F is the total nondimensionalized free energy. The nondimensionalized atomic density for component i, n_i, is defined by

$$n_i = \frac{\rho_i - \rho_{i,0}}{\rho_{i,0}}, \tag{3}$$

where ρ_i is the actual atomic number density and $\rho_{i,0}$ is the reference atomic number density. In general, F_A and F_B could be any one-component free-energy model, with either three-point [23,41,42] or only two-point [18,19] interactions. For

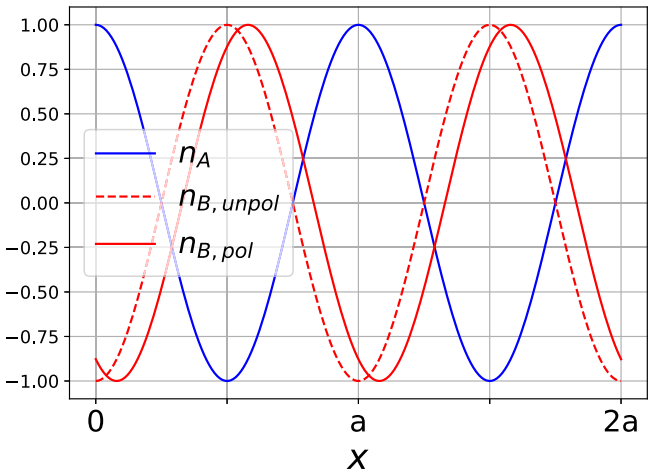

FIG. 2. Schematic of polarization in one dimension. In the unpolarized state, the n_A (blue) and n_B (red dashed) curves are exactly 180° out of phase. When the system polarizes, n_B shifts (red solid).

simplicity, in this article $F_A[n_A]$ and $F_B[n_B]$ will be identical XPFC models in the form of Eq. (1) [17,18]. The correlation function itself is defined in Fourier space such that

$$\hat{C}_A(q) = \hat{C}_B(q) = \max_j \left[b_j e^{\frac{-(q-q_j)^2}{2\sigma_j^2}} \right], \tag{4}$$

where $\hat{C}_i$ is the Fourier transform of the isotropic two-point correlation function for component i, $q = |\boldsymbol{q}|$, q_j are constants that determine the crystal structure, σ_j are standard deviations that control the elastic constants, and b_j are positive numbers connected to the system temperature [18].

A. Symmetric transitions

The simplest method for modeling exact intermetallics is to, following Taha *et al.*, Taylor expand F_{AB} in the variables n_A and n_B. To fourth order, for the symmetric n_A and n_B components

$$F_{AB} = \int_V \left[\alpha_2 n_A n_B + \alpha_3 \left(n_A n_B^2 + n_A^2 n_B \right) + \frac{\alpha_4}{2} n_A^2 n_B^2 + \alpha_5 \left(n_A^3 n_B + n_A n_B^3 \right) \right] d\boldsymbol{r}. \tag{5}$$

For additional simplicity, $\alpha_5 = 0$ henceforth. To explain why Eq. (5) is sufficient for polarization, Landau models for the one-dimensional (1D) and two-dimensional cases will be explained.

1. One-dimensional crystal

Consider the case where the single-component correlation function [Eq. (4)] is only a single Gaussian with a peak at wave number $q_1 = 2\pi/a$, where a is the lattice constant. In one dimension, the polarization imagined is shown in Fig. 2. The blue and red curves are the same shape but are phase shifted relative to each other. In the unpolarized state, the relevant phase shift, Δx, between the two waves is exactly $a/2$. In the polarized state on the other hand, the phase shift $\Delta x = a/2 + \delta$, where δ is the nonzero displacement from the centrosymmetric position.

The conditions for this displacive phase transition can be understood with one-dimensional Landau theory. Since the single-component correlation function contains only a single peak, it is reasonable to use a one mode expansion for n_i. Namely,

$$n_A(x) = \bar{n}_A + Ae^{iq_1 x} + A^* e^{-iq_1 x} \tag{6}$$

and

$$n_B(x) = \bar{n}_B + Be^{iq_1 x} + B^* e^{-iq_1 x}, \tag{7}$$

where A and B are the amplitudes, A^* and B^* are the complex conjugates of A and B, and $\bar{n}_A = \bar{n}_B$ to ensure charge neutrality. For the duration of this article, $\bar{n}_A = 0$ for simplicity. Since $F[n_A, n_B] = F[n_B, n_A]$, it is assumed that $|A| = |B|$. This is equivalent to assuming that n_B is a phase-shifted copy of n_A. Consequently, B can be expressed as

$$B = Ae^{iq_1 \Delta x}. \tag{8}$$

Since F_A and F_B are independent of Δx, only Eq. (5) must be minimized to find the conditions for polarization. Plugging in Eq. (6) and Eq. (7) into Eq. (5) in the simplified $\alpha_3 = 0$ case results in

$$\frac{F_{AB}}{a} = -2\alpha_2 |A|^2 \cos(q_1 \delta) + \alpha_4 |A|^4 [2 + \cos(2q_1 \delta)]. \tag{9}$$

From Eq. (9) it is clear why α_4 is necessary; without it, $\delta = 0$ or $\delta = a/2$ (depending on the sign of α_2). The polarization phenomena occurs because with $\alpha_2 > 0$, the $n_A n_B$ term favors $\delta = 0$ while the $n_A^2 n_B^2$ term favors $\delta = \pm a/4$. This competition drives a displacive phase transition. More precisely, there is polarization when $\alpha_2, \alpha_4 > 0$ and

$$\frac{\alpha_2}{\alpha_4 |A|^2} < 2, \tag{10}$$

with the value of the displacement itself being

$$\delta = \frac{1}{q_1} \cos^{-1} \frac{\alpha_2}{2\alpha_4 |A|^2}. \tag{11}$$

The polarization condition, Eq. (10), can also be derived by Taylor expanding Eq. (9)

$$\frac{F_{AB}}{a|A|^2} \approx (-2\alpha_2 + 3\alpha_4 |A|^2) + q_1^2 (\alpha_2 - 2\alpha_4 |A|^2)\delta^2 + q_1^4 \left(-\frac{\alpha_2}{12} + \frac{2}{3}\alpha_4 |A|^2 \right) \delta^4. \tag{12}$$

As usual for a single-order-parameter quartic Landau model, the equilibrium phase just depends on the sign of the quadratic term.

2. Two-dimensional polarization

Unlike in one dimension, in two dimensions there are many possible polarization directions. In this work, only a square crystal is considered for simplicity. In the unpolarized state [Fig. 1(a)], the phase shift, $\Delta \boldsymbol{r}$, between n_A and n_B is $(a/2, a/2)$. In the polarized state [Fig. 1(b)–1(d)], the n_B peaks are off-center, i.e., $\boldsymbol{\delta} = \Delta \boldsymbol{r} - (a/2, a/2) = (\delta_x, \delta_y)$ is nonzero.

To understand the polarization process, Landau theory analysis like in 1D is performed. Unfortunately, it is more difficult. Since the square crystal structure is two dimensional and cannot be stabilized by a single frequency [17,18], now n_i are expressed as more general Fourier series. Namely

$$n_A(\boldsymbol{r}) = \sum_{hk} A_{hk} e^{i\boldsymbol{q}_{hk}\cdot\boldsymbol{r}} \tag{13}$$

and

$$n_B(\boldsymbol{r};\Delta\boldsymbol{r}) = \sum_{hk} A_{hk} e^{i\boldsymbol{q}_{hk}\cdot(\boldsymbol{r}+\Delta\boldsymbol{r})}, \tag{14}$$

where

$$\boldsymbol{q}_{hk} = h\hat{\boldsymbol{b}}_1 + k\hat{\boldsymbol{b}}_2 \tag{15}$$

is a reciprocal lattice vector of the crystal, h and k are integers, and $\hat{\boldsymbol{b}}_i$ is the ith primitive reciprocal lattice vector. It is worth noting that during numerical simulations, it was discovered that the approximation of Eq. (8) and Eq. (14) is not exactly true. Meaning n_B is not exactly a phase-shifted copy of n_A, and given the numerical n_A, there is no $\Delta\boldsymbol{r}$ that exactly solves Eq. (14) for all amplitudes. For simplicity, however, the approximation that a single parameter, the phase-shift vector $\Delta\boldsymbol{r}$, can map A_{hk} to B_{hk} is made.

In addition to the phase-shift approximation, there are other complications when converting this model into a Landau model like in one dimension. Since the unpolarized state is a member of the plane group $p4mm$, there are eight general Wyckoff positions denoting equivalent positions in the unit cell, and these real-space symmetries correspond to symmetries in the amplitudes [43]. If the Fourier series in Eq. (13) has its origin at the corner of a unit cell, then one example equivalency is that

$$n_A(x,y) = n_A(x,-y) \Rightarrow A_{hk} = A_{h\bar{k}}. \tag{16}$$

This analysis for all Wyckoff positions implies that all $A_{\{hk\}}$ are equal, where $\{\cdot\}$ denotes a family of hk pairs created by the permutation and negation of the internal elements (e.g., $\{12\}$ includes eight pairs: $12, \bar{1}2, 1\bar{2}, \bar{1}\bar{2}, 21, \bar{2}1, 2\bar{1}, \bar{2}\bar{1}$). When the structure polarizes in the [10] direction, however, the plane group changes to $p1m1$. This plane group has only two general Wyckoff positions, and the only amplitude symmetry is that $A_{hk} = A_{\bar{h}k}$. Consequently, $A_{10} = A_{\bar{1}0}$ but $A_{10} \neq A_{01}$ in general, which further complicates the analytical free-energy expression. For simplicity, however, this complication is neglected as $A_{10} \approx A_{01}$ still.

With these caveats, the bulk analytical free energy, F_{AB}, as a function of two modes $A_1 = A_{\{10\}}$ and $A_2 = A_{\{11\}}$ with $\alpha_3 = \alpha_4 = 0$, is

$$\begin{aligned}\frac{F_{AB}}{\alpha_2\mathcal{A}} &= -2A_1^2[\cos(q_1\delta_x) + \cos(q_1\delta_y)] \\ &\quad + 2A_2^2\{\cos[q_1(\delta_x+\delta_y)] + \cos[q_1(\delta_x-\delta_y)]\},\end{aligned} \tag{17}$$

or, in Taylor expanded form,

$$\begin{aligned}\frac{F_{AB}}{\alpha_2\mathcal{A}} &= 4\big(-A_1^2 + A_2^2\big) + q_1^2\big(A_1^2 - 2A_2^2\big)\big(\delta_x^2+\delta_y^2\big) \\ &\quad + q_1^4\left(-\frac{1}{12}A_1^2 + \frac{A_2^2}{6}\right)\big(\delta_x^4+\delta_y^4\big) + q_1^4A_2^2\delta_x^2\delta_y^2,\end{aligned} \tag{18}$$

TABLE I. Table of parameter values for {10} polarizing model.

Quantity	Value
b_1	1.0
b_2	0.98
q_1	2π
q_2	$2\pi\sqrt{2}$
σ_1	2.0
σ_2	2.0
α_2	0.01
α_3	0.05
α_4	0.05
α_5	0
a_0	1.0
$\bar{n}$	0

$$\begin{aligned}&= F_{AB,0} + \frac{1}{2}\alpha\big(\delta_x^2+\delta_y^2\big) \\ &\quad + \frac{1}{4}\big[\Gamma_{11}\big(\delta_x^4+\delta_y^4\big) + \Gamma_{12}\delta_x^2\delta_y^2\big],\end{aligned} \tag{19}$$

where $F_{AB,0}$, α, Γ_{11}, and Γ_{12} are defined as the corresponding coefficients in Eq. (18). Equation (19) is exactly the fourth-order Landau free energy for a two-component spin system with cubic anisotropy [44]. Normally when constructing phenomenological Landau models, one must be careful to only include the terms that have the same symmetries as the crystal under study. Because the PFC model has the crystal structure built in, the resulting Landau model automatically contains only the terms with the correct symmetries.

Landau theory can be used to understand not only the existence of displacive phase transitions but also their direction. In Eq. (19), if $\Gamma_{12} > 2\Gamma_{11}$, then if polarization occurs it will be in the $\langle 10\rangle$ direction [44] ($\langle\cdot\rangle$ denotes a family of real variables in the same manner that $\{\cdot\}$ denotes a family of reciprocal space variables). If $\Gamma_{12} < 2\Gamma_{11}$, on the other hand, then any polarization will be in the $\langle 11\rangle$ direction [44]. Parameters were found such that both the $\langle 11\rangle$ [Fig. 1(c)] and $\langle 10\rangle$ [Fig. 1(b)] polarizations occur in numerical simulation, using $\alpha_3 = 0$ and $\alpha_3 \neq 0$, respectively (Table I). In the normal parameter space of the single-component PFC model, the quadratic coefficient α in Eq. (19) is always positive, so polarization does not occur. Parameters that analytically minimize the free energy and give $\langle 10\rangle$ polarizations do exist but require $\alpha_3, \alpha_4 \neq 0$ and an $A_{\{20\}}$ mode. For brevity, this full expression is emitted.

B. Generic polarization

In order to model polarization in an arbitrary direction, the free energy

$$F_{AB} = \int_V n_A^m C_{AB} * n_B^m d\boldsymbol{r}, \tag{20}$$

where m is a positive integer, is used in place of Eq. (5). The possibility of a displacive phase transition to an "arbitrary" direction is motivated by the fact that although such a polarization is impossible in fourth-order Landau theory, it is possible in eighth-order Landau theory [44]. Equation (20) itself is phenomenologically motivated, and presumably,

additional terms where the powers for n_A and n_B are not the same could give rise to additional behavior. In the simple case of a displacive transition in the square crystal, this term is sufficient to describe *all* possible polarization states consistent with the plane group. Substituting Eqs. (13) and (14) into Eq. (20) gives

$$\frac{F_{AB}(\Delta \boldsymbol{r})}{\mathcal{A}} = \sum_{h_1 k_1,\ldots,h_m k_m,\mathfrak{h}_1\mathfrak{K}_1,\ldots,\mathfrak{h}_m\mathfrak{K}_m} \prod_{\alpha=1}^{m} A_{h_\alpha k_\alpha} A_{\mathfrak{h}_\alpha \mathfrak{K}_\alpha} \times \hat{C}_{AB}(s) e^{i\boldsymbol{s}\cdot\Delta\boldsymbol{r}} \delta_{-\boldsymbol{s},\boldsymbol{t}}, \tag{21}$$

where the n_A sum has hk indices, the n_B sum has $\mathfrak{h}\mathfrak{K}$ indices,

$$\boldsymbol{s} = \sum_{l=1}^{m} \boldsymbol{q}_{\mathfrak{h}_l \mathfrak{K}_l}, \boldsymbol{t} = \sum_{l=1}^{m} \boldsymbol{q}_{h_l k_l}, \tag{22}$$

and $s = |\boldsymbol{s}|$. If n_i are Fourier expanded with two amplitudes as in Sec. IIA2, then Eq. (21) simplifies to

$$\frac{F_{AB}(\Delta \boldsymbol{r})}{\mathcal{A}} = \sum_{s} c_s e^{i\boldsymbol{s}\cdot\Delta\boldsymbol{r}}, \tag{23}$$

where

$$c_s = \sum_{K=0}^{2m} A_1^K A_2^{2m-K} N_{s,K} \hat{C}_{AB}(|\boldsymbol{s}|) \tag{24}$$

and $N_{s,K}$ is the number of vector sums in Eq. (21) such that both $\boldsymbol{s} = -\boldsymbol{t}$ and exactly K vectors of magnitude q_1 are terms in the sum $\boldsymbol{s}$. Because $N_{s,K}$ is an integer, it can be calculated exactly, albeit with computational assistance.

Observe that Eq. (23) is in the form of a Fourier series and has the same periodicity as F_A and F_B. Since $\boldsymbol{s}$ is a sum of reciprocal lattice vectors, it is a reciprocal lattice vector as well and can be referenced with indices hk. Although for finite m there are only a finite set of $\boldsymbol{s}$ vectors, as $m \to \infty$, $\boldsymbol{s}$ comes to include all reciprocal lattice vectors. Consequently, in order to create a desired $F_{AB}(\Delta \boldsymbol{r})$, one simply needs to control c_s, which is accomplished through modifying $\hat{C}_{AB}(s)$.

The fact that $\hat{C}_{AB}$ is isotropic limits F_{AB} to functions with certain types of symmetries. Since $N_{\{hk\},K}$ are all equal, $c_{\{hk\}}$ are all equal as well. This implies that F_{AB} must be a member of the $p4mm$ plane group for similar reasons as explained in Sec. IIA2. Further, if vectors $\boldsymbol{s}_{hk}$ and $\boldsymbol{s}_{uv}$ are distinct but of the same magnitude, meaning $(uv) \notin \{hk\}$ but

$$h^2 + k^2 = u^2 + v^2, \tag{25}$$

then

$$\frac{c_{hk}}{c_{uv}} = \frac{\sum_{K=0}^{2m} A_1^K A_2^{2m-K} N_{hk,K}}{\sum_{K=0}^{2m} A_1^K A_2^{2m-K} N_{uv,K}}, \tag{26}$$

since their correlation function terms must be equal. An example of coefficients that must satisfy Eq. (26) are $c_{\{34\}}$ and $c_{\{50\}}$, as well as any other Pythagorean triple. In technical terms, Eq. (25) is a Diophantine equation (whose general solution is known) [45]. However, given these restrictions on allowed F_{AB} functions and ignoring the problematic terms that solve Eq. (25), F_{AB} is controlled by setting $\hat{C}_{AB}$ according to

$$\hat{C}_{AB,\mathrm{set}}(s) = \frac{c_s}{\sum_{K=0}^{2m} A_1^K A_2^{2m-K} N_{s,K}}. \tag{27}$$

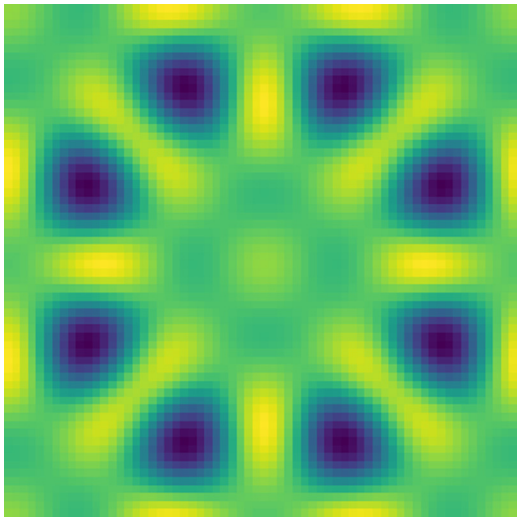

FIG. 3. F_{AB} plot over a unit cell for a desired $\boldsymbol{\delta} = (0.16, 0.34)$. The color map goes from dark blue (lowest values) to light yellow (highest values). F_{AB} contains eight equal minima as intended; horizontal, vertical, and diagonal mirror planes; as well as various fourfold rotation axes.

In order to validate that this method can create arbitrary polarizations, it is necessary to choose c_s values. As a simple test, these coefficients were chosen to be the coefficients from an expansion of a sum of delta functions that have the eightfold symmetry required by a generic position in the $p4mm$ plane group [43]. Namely,

$$c_{hk}(x_0, y_0) = \cos[2\pi(hx_0 + ky_0)] + \cos[2\pi(hx_0 - ky_0)] + \cos[2\pi(hy_0 + kx_0)] + \cos[2\pi(hy_0 - kx_0)], \tag{28}$$

where $\Delta \boldsymbol{r} = (x_0, y_0)$ (in units of the lattice constant). Although in general A_1 and A_2 are functions of F_{AB}, this makes calculation of $\hat{C}_{AB,\mathrm{set}}$ challenging. An example F_{AB} plot for $(x_0, y_0) = (0.66, 0.84)$ is shown in Fig. 3, where the single-component amplitudes are used for A_i as in approximation, which is reasonable when F_{AB} is small.

Since Eq. (27) only specifies the value of $\hat{C}_{AB}$ at points, a simple extension of Eq. (4) is used for defining $\hat{C}_{AB}(q)$. Namely,

$$\hat{C}_{AB}(q) = \max_j \left[\mathfrak{b}_j e^{\frac{-(q-\mathfrak{q}_j)^2}{2\varsigma_j^2}}\right] + \min_j \left[B_j e^{\frac{-(q-Q_j)^2}{2\varsigma_j^2}}\right], \tag{29}$$

where

$$\mathfrak{b}_j = \Omega \hat{C}_{AB,\mathrm{set}}(\mathfrak{q}_j)$$
$$B_j = \Omega \hat{C}_{AB,\mathrm{set}}(Q_j), \tag{30}$$

$\hat{C}_{AB,\mathrm{set}}(\mathfrak{q}_j) > 0$, $\hat{C}_{AB,\mathrm{set}}(Q_j) < 0$, and Ω is a scale factor. In the limit where ς is small, Eq. (29) reduces to a sum. The parameters listed in Table II were successfully used to create the displacement in Fig. 1(d).

Note that since $\hat{C}_{AB}$ is isotropic, the strain energy is proportional to the displacement squared. If the displacement is interpreted as a polarization, this is consistent with the

TABLE II. Table of parameter values for crystal with $\boldsymbol{p} = (0.16, 0.34)$. The associated set of $\{hk\}$ pairs is given for each reciprocal wave-vector magnitude.

Quantity	Value	Vector set
$\mathfrak{q}_1$	$2\pi\sqrt{8}$	{22}
$\mathfrak{q}_2$	$2\pi\sqrt{10}$	{31}
$\mathfrak{q}_3$	$2\pi\sqrt{20}$	{24}
Q_1	$2\pi\sqrt{2}$	{11}
Q_2	4π	{20}
Q_3	8π	{40}
Q_4	$2\pi\sqrt{18}$	{33}
m	4	
$\mathfrak{b}_1$	7.6531×10^{-4}	
$\mathfrak{b}_2$	6.3636×10^{-3}	
$\mathfrak{b}_3$	1.2671×10^{-1}	
B_1	2.6224×10^{-4}	
B_2	5.2784×10^{-4}	
B_3	6.3886×10^{-2}	
B_4	1.7314×10^{-1}	
ς	0.1	
a_0	1.0	
$\bar{n}$	0	

electrostriction effect. Strain energies proportional to the polarization are also possible, i.e., the piezoelectric effect, but only if $\hat{C}_{AB}$ is anisotropic, for example, if

$$F_{AB} = \int_V n_A \frac{\partial n_B}{\partial x}. \tag{31}$$

C. Dynamics

In order to create dynamic models from these free energies, the standard conserved local dynamics equations were employed [16]. Namely,

$$\frac{\partial n_i}{\partial t} = \nabla^2 \frac{\delta F}{\delta n_i}. \tag{32}$$

In cases where the goal is to minimize the free energy, and the path to equilibrium is not of interest, the global dynamics equation,

$$\frac{\partial n_i}{\partial t} = -\frac{\delta F}{\delta n_i} + \frac{1}{V}\int_V \frac{\delta F}{\delta n_i} d\boldsymbol{r}, \tag{33}$$

can be used instead for computational efficiency [46].

III. COMPARISON TO LGD MODELS

Like traditional PFC models [47], the DPFC model can be mapped to phase-field models, namely Landau-Ginzburg-Devonshire models. In general, these models are of the form

$$F = \int_V [f_{\text{bulk}}(\boldsymbol{p}) + f_{\text{grad}}(\nabla \boldsymbol{p}) + f_{\text{elast}}(\epsilon) + f_c(\boldsymbol{p}, \epsilon) + f_{\text{elec}}(\boldsymbol{p}, \boldsymbol{E})] d\boldsymbol{r}, \tag{34}$$

where f_{bulk} is the bulk free-energy density, f_{grad} is the energy due to gradients in the polarization, f_{elast} is the contribution from the strain tensor ϵ, f_c is the coupling energy between the polarization and strain fields, and f_{elec} is the electrical energy density as a result of the electric field $\boldsymbol{E}$ [37]. Mapping the DPFC model to a LGD model is of interest because LGD parameters have been calculated for real materials [33,48,49], and, consequently, this is a possible method for PFC parameters fitting.

Although the free energies in Sec. II were functions of the displacement $\boldsymbol{\delta}$, LGD models are functions of the polarization, $\boldsymbol{p}$. The connection between the displacement and the polarization is explored in Appendix A, but the upshot is that the displacement is proportional to the polarization. The derivation of the LGD model from the DPFC model is discussed below, and the analytic results for a three-amplitude approximation for n_i are found in Table III.

A. Bulk energy

The bulk, or Landau-Devonshire, free energy is derived from the DPFC in the same manner as discussed in Sec. IIA2. Three-dimensional Landau-Devonshire potentials used practically for modeling perovskites are either sixth or eighth order [50,51], and the PFC model automatically gives the correct symmetries for the bulk energy regardless of the order of the expansion. To sixth order, the free energy of a perovskite is

$$f_{\text{bulk}} = \tfrac{1}{2}\alpha\left(p_x^2 + p_y^2\right) + \tfrac{1}{4}\left[\gamma_{11}\left(p_x^4 + p_y^4\right) + \gamma_{12}p_x^2p_y^2\right] + \tfrac{1}{6}\left[\omega_{111}\left(p_x^6 + p_y^6\right) + \omega_{112}\left(p_x^4p_y^2 + p_x^2p_y^4\right)\right]. \tag{35}$$

B. Gradient energy

In LGD models for perovskites, the two-dimensional gradient term is

$$f_{\text{grad}} = \frac{1}{2}g_{11}\left(\frac{\partial {p_x}^2}{\partial x} + \frac{\partial {p_y}^2}{\partial y}\right) + g_{12}\frac{\partial p_x}{\partial x}\frac{\partial p_y}{\partial y} + g_{44}\left(\frac{\partial {p_x}^2}{\partial y} + \frac{\partial {p_y}^2}{\partial x}\right). \tag{36}$$

Although many authors include a fourth gradient coefficient [33,48,52], two of the coefficients are degenerate [35,53].

The gradient coefficients in our model are calculated by imagining that n_A is fixed, and the polarization gradients are due to the offset $\Delta\boldsymbol{r}$ between the sublattices in Eq. (14) being a slowly varying function of position. The strained reciprocal lattice vectors, $\boldsymbol{q}^{\text{str}}$, are defined in terms of the Jacobian of $\Delta\boldsymbol{r}$ (the displacement gradient tensor in the language of elasticity), $\mathfrak{u}$, and the unstrained reciprocal lattice vectors $\boldsymbol{q}$. Namely,

$$\boldsymbol{q}^{\text{str}} = (\mathfrak{u} + \mathcal{I})^{-1} \cdot \boldsymbol{q}, \tag{37}$$

where $\mathcal{I}$ is the identity matrix. If the strained wave vectors are used in Eq. (14), then the difference in free energy from the unstrained state will solely be due to the two-point correlation function of the strained component. On Taylor expanding to second order, this free-energy difference is exactly Eq. (36), where

$$g_{11} = -q_1^2\tilde{Q}^2\sum_{i=1}^{3}|A_i|^2\hat{C}''_{BB}(q_i),$$
$$g_{12} = g_{44} = -q_1^2\tilde{Q}^2|A_2|^2\hat{C}''_{BB}(q_2), \tag{38}$$

TABLE III. Table of LGD parameter values. The amplitudes are the values that minimize the DPFC free energy.

Variable	Expression
α	$-2q_1^2\tilde{Q}^2\big(6\alpha_4A_1^4 - A_1^2\big(\alpha_2 + 20\alpha_4A_2^2 + 32\alpha_4A_3A_2 - 4\alpha_3A_3 + 40\alpha_4A_3^2\big) + 2\big\{6\alpha_4A_2^4 + A_2^2[\alpha_2 + 4A_3(4\alpha_3 + 9\alpha_4A_3)] + 2A_3^2\big(\alpha_2 + 6\alpha_4A_3^2\big)\big\}\big)$
γ_{11}	$\frac{1}{3}q_1^4\tilde{Q}^4\big\{12\alpha_4A_1^4 - A_1^2\big[\alpha_2 + 4\big(11\alpha_4A_2^2 + 32\alpha_4A_3A_2 - 7\alpha_3A_3 + 58\alpha_4A_3^2\big)\big] + 2\big[24\alpha_4A_2^4 + A_2^2\big(\alpha_2 + 204\alpha_4A_3^2 + 40\alpha_3A_3\big) + 8A_3^2\big(\alpha_2 + 12\alpha_4A_3^2\big)\big]\big\}$
γ_{12}	$4q_1^4\tilde{Q}^4\big[8\alpha_4A_2^4 + A_2^2\big(\alpha_2 - 16\alpha_4A_1^2 + 8\alpha_3A_3 + 76\alpha_4A_3^2\big) + 4A_1^2A_2(\alpha_3 - 6\alpha_4A_3) + 2\alpha_4\big(A_1^2 - 4A_3^2\big)^2\big]$
ω_{111}	$-\frac{1}{60}q_1^6\tilde{Q}^6\big[36\alpha_4A_1^4 - A_1^2\big(\alpha_2 + 4\big(35\alpha_4A_2^2 + 128\alpha_4A_3A_2 - 31\alpha_3A_3 + 430\alpha_4A_3^2\big)\big) + 2\big(96\alpha_4A_2^4 + A_2^2(\alpha_2 + 4A_3(34\alpha_3 + 399\alpha_4A_3)) + 32A_3^2(\alpha_2 + 36\alpha_4A_3^2)\big)\big]$
ω_{112}	$\frac{1}{3}q_1^4\tilde{Q}^6\big\{12\alpha_4A_1^4 - A_1^2\big[\alpha_2 + 4\big(11\alpha_4A_2^2 + 32\alpha_4A_3A_2 - 7\alpha_3A_3 + 58\alpha_4A_3^2\big)\big] + 2\big[24\alpha_4A_2^4 + A_2^2\big(\alpha_2 + 204\alpha_4A_3^2 + 40\alpha_3A_3\big) + 8A_3^2\big(\alpha_2 + 12\alpha_4A_3^2\big)\big]\big\}$
c_{11}	$2\big[\alpha_2 + A_1^2\big(-4\alpha_4 + \frac{b_1q_1^2}{\sigma_1^2} + 4\big) + A_2^2\big(12\alpha_4 + \frac{b_2q_1^2}{\sigma_2^2} + 4\big) + 1\big]$
c_{12}	$\frac{2A_2^2b_2q_1^2}{\sigma_2^2}$
c_{44}	$2\alpha_2 - 8\alpha_4A_1^2 + 24\alpha_4A_2^2 + 24\alpha_4A_3^2 + \frac{2A_2^2b_2q_1^2}{\sigma_2^2} + 8A_1^2 + 8A_2^2 + 8A_3^2 + 2$
g_{44}	$\frac{A_2^2b_2q_1^2\tilde{Q}^2}{\sigma_2^2}$
g_{12}	$\frac{A_2^2b_2q_1^2\tilde{Q}^2}{\sigma_2^2}$
g_{11}	$q_1^2\tilde{Q}^2\big(\frac{A_1^2b_1}{\sigma_1^2} + \frac{A_2^2b_2}{\sigma_2^2} + \frac{A_3^2b_3}{\sigma_3^2}\big)$
$\tilde{Q}$	$-\frac{e}{a}$

and $\tilde{Q}$ is the proportionality constant connecting displacement to polarization. This method for calculating the gradient coefficients is similar to how elastic constants were originally calculated for a single-component PFC model [40]. It was later discovered that this method for calculating elastic constants is incorrect since the average density changes when the system is strained [54,55]. This critique could also be leveled against this method of calculating the gradient coefficients. However, because the electrostriction coefficients for this model are approximately zero (see Sec. III C), density changes as a function of polarization can be ignored.

C. Elastic energy

In addition to the free energies due to polarizations, there are also free energies due to elastic strain. For a material with cubic symmetry, the elastic energy in two dimensions is

$$f_{\text{elast}} = \tfrac{1}{2}c_{11}\big(\epsilon_{xx}^2 + \epsilon_{yy}^2\big) + c_{12}\epsilon_{xx}\epsilon_{yy} + 2c_{44}\epsilon_{xy}^2. \tag{39}$$

The elastic constants are derived in the manner suggested by Wang *et al.* [55], except the anisotropic variations of the amplitudes are neglected for simplicity. In order to avoid issues with the stresses inherent in the undeformed state affecting the elastic constants, the system pressure is set to zero in the calculations. Namely, a linear term $\int_V \beta(n_A + n_B)d\boldsymbol{r}$ is added to the free energy, Eq. (2), and β is then solved so the system pressure is zero.

In real materials, in addition to the purely elastic strain, the f_c energy couples the polarization and strain fields. Namely, there are terms of the form $-\lambda_{ijkl}\epsilon_{ij}p_kp_l$, where λ is the electrostrictive constant tensor [37]. The result of these terms are that the spontaneous polarization causes a plastic strain so that the unit cell shape changes. For example, $PbTiO_3$ undergoes a cubic $\rightarrow$ tetragonal transition when polarization occurs. Indeed, numerical simulations of the polarization process verifies a square $\rightarrow$ rectangular transition. However, this phenomenon, unlike in real systems, is very small. Using the coefficients in Table I as a test case, the unit cell distortion $c/a \simeq 1.0003$. Because the distortion is so small, the electrostriction constants are approximately zero in this work.

D. Electrostatic energy

The free energy due to the electrical energy density, f_{elec}, is also important [33,35,37,49,56,57] and does not arise from any of the DPFC terms. Part of the problem is that the electrical energy is a function of the charge density, and the charge density is not uniquely defined by the atomic density profile alone. One possibility is to assume that A has a positive charge, B an equal and opposite charge, and there are no other charge sources. In this case, the charge density $\rho_e \propto n_A - n_B$, and the PFC electrostatic energy is

$$F_{\text{elec}} = \frac{w}{2}\int |\nabla\varphi|^2 d\boldsymbol{r}, \tag{40}$$

where φ is the electric potential from Gauss's law and w is some constant. Because of the lack of strong core repulsions in Eq. (5), when w is large, the atoms overlap to reduce the electrical energy, i.e., $n_A = n_B$. On the other hand, when w is small, the inclusion of this electrostatic energy did not appear to make any qualitative difference for simulations with periodic boundary conditions.

Consequently, this work neglects the contributions of f_{elec} for simplicity, which corresponds to the limit of high dielectric constant. Neglecting f_{elec} is in fact what early LGD models

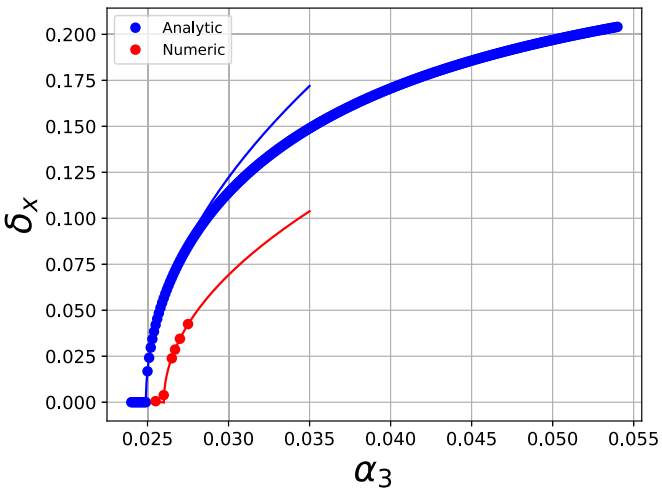

FIG. 4. Second-order phase transition calculated numerically [Eq. (5)] and analytically [Eq. (36)]. The lines are power-law fits with exponents 1/2.

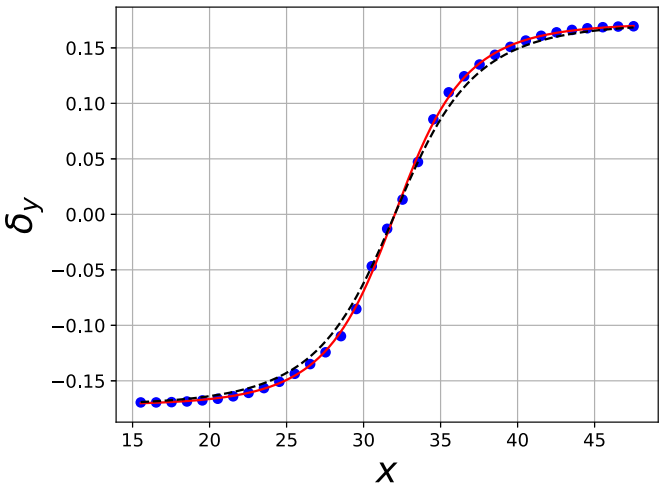

FIG. 5. Displacement in the y direction across an Ising wall. The points are the numerically calculated values, the red line is a fit to Eq. (43) with $\xi = 7.26$, and the dashed line is the analytically calculated $\xi = 8.23$ width. As explained in Appendix A, $\delta_y \propto p_y$.

did as well [48,52,58], and explicit electrostatic contributions as well as external fields are left for future work.

IV. APPLICATIONS

A. Phase transitions

As a method for comparing the full numerical model to the analytic LGD theory, a ⟨10⟩ displacive phase transition was examined near the critical temperature. As predicted by fourth-order Landau theory [44], the displacive phase transition is second order. As can be seen in Fig. 4, the numerical and analytical results match closely. This check can be thought of as a verification of the Landau-Devonshire [Eq. (35)] portion of the free energy.

Of course, displacive phase transitions can be both first and second order. It is possible to change the order of the phase transition by including higher-order couplings than Eq. (5), for example, letting

$$F_{AB} = \int_V \left(\alpha_2 n_A n_B + \alpha_4 n_A^2 n_B^2 + \alpha_6 n_A^3 n_B^3\right) d\boldsymbol{r}. \tag{41}$$

This can be proved using the same method of analysis as Sec. IIA1. For simplicity, however, first-order applications are omitted and the parameters used for generating Fig. 4 are used for the rest of Sec. IV, which only permit ⟨10⟩ polarizations. These values are in Table I.

B. Domain walls

As a method for comparing the polarization gradient coefficients in our numerical model to the analytic LGD theory, an isolated domain wall was numerically modeled. The system was tested numerically in a 64×2 domain with periodic boundary conditions and domain walls at the center and edges of system. The method for calculating the displacements is described in Appendix B. Compared with the Cahn-Hilliard equation, many more types of domain walls are possible in our system, including $\uparrow\downarrow$, $\uparrow\rightarrow$, and $\rightarrow\leftarrow$ boundaries. In the case of the $\uparrow\downarrow$ walls simulated, known as Ising walls [59], the math reduces to the one-dimensional case. For a sixth-order bulk free energy, the analytic profile is

$$p_y(x) = p_0 \frac{\sinh\left(\frac{x-x_0}{\xi}\right)}{\left[C + \sinh^2\left(\frac{x-x_0}{\xi}\right)\right]^{1/2}}, \tag{42}$$

where

$$\xi = \frac{1}{2p_0}\sqrt{\frac{g_{44}}{C(120\omega_{111}p_0^2 + 3\gamma_{11})}} \tag{43}$$

measures the interface width and C measures the contribution of the sixth-order bulk energy term (the typical fourth-order tanh profile occurs when $C = 1$) [60]. By fitting the results of the numerical domain wall to Eq. (42), ξ and C were calculated, and their values were used to make a seminumeric estimate of g_{44} (Fig. 5). Namely, the value of p_0 from a numerical bulk polarization equilibration; A_1, A_2, and A_3 from a numerical bulk unpolarized state equilibration; and ω_{111} and γ_{11} from the LGD model were combined with $\xi = 7.26$ and $C = 0.41$ from Ising wall simulation to yield $g_{44} = 0.19$. In comparison, the expression for g_{44} from the LGD model (Table III) is $g_{44} = 0.24$. This implies that the method for calculating the polarization gradient energy coefficient is somewhat reasonable.

C. Quadrijunctions

In "traditional" systems, such as soap froths and single-phase grain structures, quadrijunctions (junctions where four domain walls meet) are thermodynamically unstable and split into trijunctions [61,62]. However, Cahn showed that in a system similar to ours—an Ising-type stripe formation model on a discrete, square lattice with two components—that weak first and strong second-neighbor interactions stabilized quadrijunctions [62]. Although quadrijunctions have not been studied using LGD models to the authors' knowledge, it was thought that the DPFC model might stabilize quadrijunctions

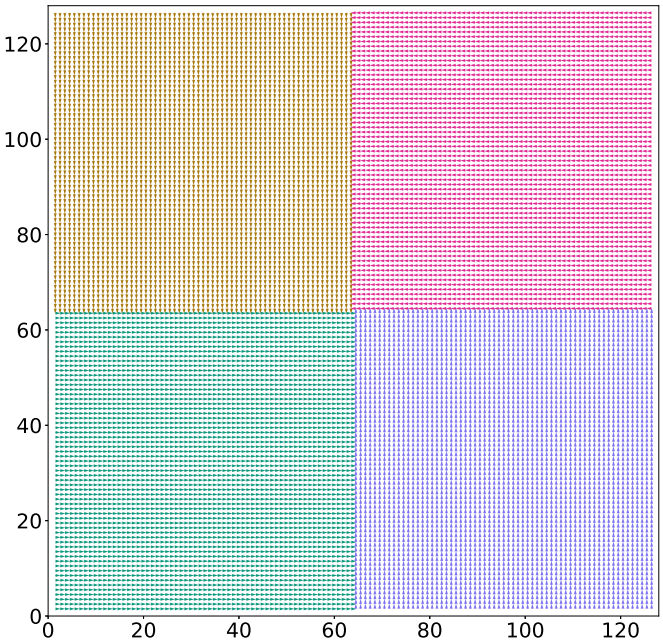

(a)

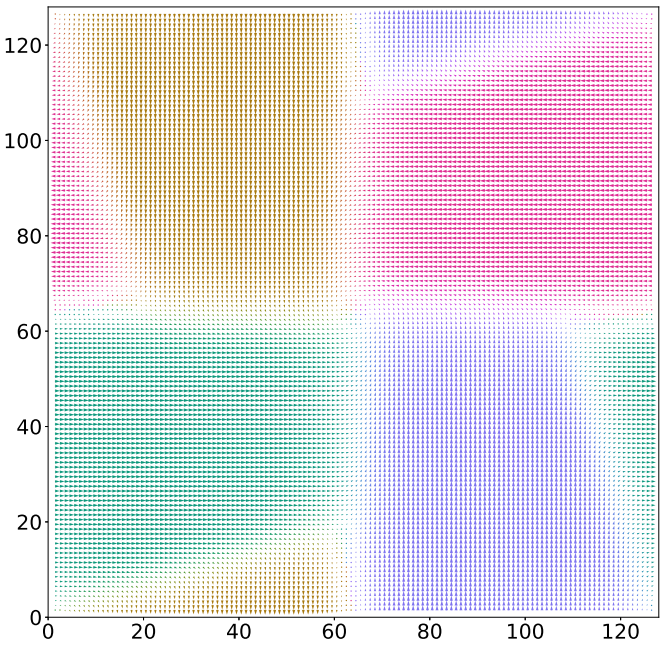

(b)

FIG. 6. The colors denote the four different polarization directions: [10], [01], [$\bar{1}$0], and [0$\bar{1}$]. The white regions are domain boundaries, and the axes are labeled in units of the lattice constant. (a) The initial condition, with spiraling quadrijunctions at the corners and center, and nonspiraling quadrijunctions at the midpoints of the sides. (b) The system a short simulated time afterward. The spiraling quadrijunctions remain stable, but the nonspiraling quadrijunctions have decomposed into two trijunctions.

since. like in Cahn's Ising model, there are four possible domains.

This hypothesis was confirmed by simulating a 128 × 128 periodic domain with clockwise spiraling quadrijunctions ($\begin{smallmatrix}\uparrow & \rightarrow\\ \leftarrow & \downarrow\end{smallmatrix}$) at the system's center and corners and head-to-head nonspiraling quadrijunctions ($\begin{smallmatrix}\uparrow & \leftarrow\\ \rightarrow & \downarrow\end{smallmatrix}$) at the edges (Fig. 6). A large system size was used to minimize the possibility of finite-size effects. The nonspiraling quadrijunctions quickly decomposed into trijunctions, but the spiraling junctions remained stable. This is somewhat surprising, as although head-to-head boundaries do not exist in real systems, this is attributed to an excess charge accumulation at the interface, and our model lacks explicit electrostatics terms [60].

D. Domain coarsening with dislocations

Although it is possible to simulate polarization domains through LGD models [37], it is challenging to study the interaction of polarizations with dislocations and grain boundaries using LGD models or traditional atomistic methods. In contrast, this is possible using the DPFC model.

As an illustrative example, domain coarsening across a low-angle symmetric grain boundary was simulated. First, the low-angle boundary was initialized by using a plane-wave expansion in the form of Eq. (6) for n_i, and the standard method was implemented for calculating the dimensions of the periodic grains [46]. The maxima of the n_B plane-wave expansion were then located. A random number from a multivariable normal distribution was subsequently generated and added to the stored position for the maxima. The plane-wave version of n_B was then discarded, and a new n_B that was the sum of multivariable Gaussians was created, with each Gaussian centered on a moved maxima. In this way, a system was generated such that the polarization in each unit cell was random.

This system was then evolved using the dynamics of Eq. (32), and the results are in Fig. 7. The central line of dislocations clearly impedes the motion of the central [10] domain. Additionally, the [0$\bar{1}$] region on the left grows downward, despite this increasing the amount of interface. It is thought that this occurs because the two interfaces created are lower in energy than the single one is destroys, consistent with $g_{44}, g_{12} < g_{11}$. Neither of these behaviors are motion by mean curvature.

V. SUMMARY

The DPFC model provides a simple and computationally efficient way to begin incorporating ferroelectricity into the PFC model. It is possible to compare this model to LGD models and get qualitatively reasonable results, and phenomena that would be very challenging otherwise, such as the interaction of dislocations with grain boundaries, can begin to be studied. Given a suitable simple cubic model, the model could also be extended to three dimensions, and more complex displacive transitions, such those accomplished through octahedral rotations in $SrTiO_3$ [51], might also be possible. Because of the important similarities between ferroelectric and martensitic transformations, this paper could also form the basis for a PFC model of the latter. Additionally, the ideas introduced when creating "generic" displacements begins the conversation about how one might model truly complex materials, such as metal-organic frameworks, using the phase-field crystal method.

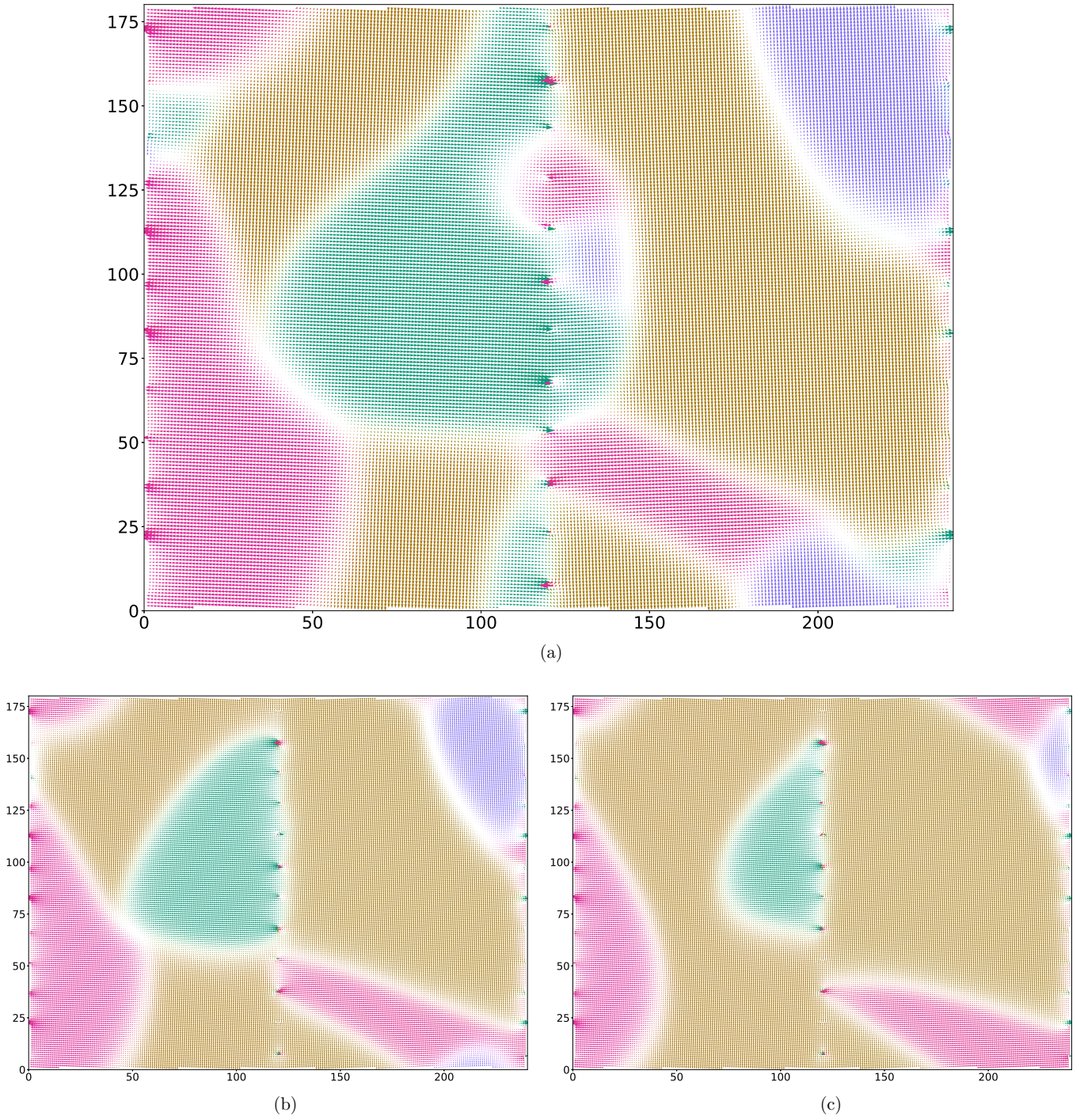

FIG. 7. Polarization domain coarsening across a 3.8° tilt grain boundary at 9000 (a), 23 000 (b), and 48 000 (c) timesteps. The color scheme and units are the same as for Fig. 6. The dislocations are recognizable as the line of strangely colored points down the middle and edges of the figures. The dislocations impede the domain boundary motion of the central [10] domain. Further, the $[0\bar{1}]$ region on the left side grows in (a)–(c), despite this growth increasing the amount of boundary. The reason for this is hypothesized to be because ←→ interfaces are higher energy than ←↓ and ↓→ interfaces. Thus, domain motion is not simply reduction of mean curvature.

Although the DPFC successfully simulates displacive transitions, there is room for improvement with regards to its ability to simulate real perovskites. When $PbTiO_3$ undergoes a ⟨10⟩ displacive transition, it simultaneously undergoes a cubic → tetragonal transition, and $c/a = 1.18$ [63]. Although the DPFC demonstrates a square → rectangular transition, $c/a \approx 1$. The DPFC model has long-range elastic interactions, but there are no long-range electrostatic contributions. It is also not possible to alter the polarization gradient energy coefficients independent of the elastic constants. These improvements are left for future work.

ACKNOWLEDGMENTS

Zhi-Feng Huang, David Montiel, Katsuyo Thornton, and Jason Luce are thanked for many helpful discussions. The National Science Foundation Graduate Research Fellowship, NSF DMR-1507033, NSF DMR-3003700315, and Northwestern University are thanked for financial support. K.R.E. acknowledges support from the National Science Foundation under Grant No. DMR-1506634.

APPENDIX A: DISPLACEMENT AND POLARIZATION

The definition of polarization is in fact not trivial and relies on insights from the modern theory of polarization [64]. A brief introduction is given here, with the definition used in this paper given by Eq. (A10).

1. Circular mean

Given N real numbers, the mean is typically defined as

$$\bar{x} \equiv \frac{1}{N}\sum_{j=1}^{N} x_j \tag{A1}$$

in the discrete case and

$$\bar{x} \equiv \frac{1}{a}\int_0^a x\mathcal{P}(x)dx \tag{A2}$$

in the continuous case, where $\mathcal{P}(x)$, the probability density function for x, is nonzero only in the interval $[0, a]$. However, these definitions cause problems when calculating the means of angles. For most purposes, it makes more sense for the mean of 0° and 360° to not be 180°, the result of Eq. (A1), but rather 0° or 360°. Consequently, the circular mean is defined as

$$\bar{\theta} \equiv \mathrm{Im}\ln\sum_{j=1}^{N} e^{i\theta_j}. \tag{A3}$$

This equation takes angles, converts them to Cartesian coordinates on the unit circle, calculates the average of these points, and then calculates the angle for that Cartesian point. In the continuous case,

$$\bar{\theta} = \mathrm{Im}\ln\int_s^{s+2\pi} e^{i\theta}\mathcal{P}(\theta)d\theta, \tag{A4}$$

where s is any real number. The circular mean is multivalued since angles themselves are not uniquely defined.

2. Multivalued polarization

The circular mean is useful for calculating means of other periodic fields, not just angles. The dipole moment of a finite system is

$$\boldsymbol{\mu} = \int_V \boldsymbol{r}\rho_e(\boldsymbol{r})d\boldsymbol{r}, \tag{A5}$$

where $\boldsymbol{\mu}$ the dipole moment and ρ_e is the charge density. How is the dipole moment for a bulk material expressed? One commonly encountered and intuitive definition of polarization is that it is the dipole moment per unit cell. However, this results in a polarization that is origin dependent. Namely, in 1D

$$\frac{\mu}{a} = \frac{1}{a}\int_s^{s+a} x\rho_e(x)dx \tag{A6}$$

is a function of the origin s [64]. Notice, however, that Eq. (A4) is origin independent since $e^{i\theta}$ is periodic.

Drawing inspiration from this concept, in the modern theory of polarization [65,66] the polarization is defined as

$$p = \frac{\mathfrak{e}}{2\pi}\mathrm{Im}\ln\int e^{i\frac{2\pi}{a}\left(\sum_l^N Z_l x_l - \sum_j^M x_j\right)}|\psi(\boldsymbol{x})|^2 d\boldsymbol{x}, \tag{A7}$$

where $\mathfrak{e}$ is the electron charge, N is the number of nuclei, M is the number of electrons, $\mathfrak{e}Z_l$ is the charge of nucleus l, ψ is the $(N+M)$-particle wave function, and $\boldsymbol{x} = (x_1, \ldots, x_{N+M})$.

Consequently, an ideal PFC polarization model would track the electrons in the system as well as the nuclei. In our model, however, there are only the atomic densities. In order to calculate a polarization, it is assumed, as in Sec. III D, that the charge density is $\rho_e \propto (\rho_A - \rho_B)$, and it is further assumed that there are no other charges in the system. Thus, we let

$$p = \frac{e_c}{2\pi}\mathrm{Im}\ln\int_s^{s+a}\int_s^{s+a} e^{iq(x_A - x_B)}|\psi(x_A, x_B)|^2 dx_A dx_B, \tag{A8}$$

where e_c is the charge proportionality constant. It seems reasonable to guess that

$$|\psi(x_A, x_B)|^2 = \mathcal{P}(x_A, x_B) = \frac{\rho_A(x_A)}{a\bar{\rho}_A}\frac{\rho_B(x_B)}{a\bar{\rho}_B}, \tag{A9}$$

since then $\int \mathcal{P}(x_A, x_B)dx_A dx_B = 1$. However, the impact of differing assumptions deserves further research. Thus,

$$p = \frac{e_c}{2\pi}\mathrm{Im}\ln\int_s^{s+a} e^{iqx_A}\rho_A(x_A)dx_A \times \int_s^{s+a} e^{-iqx_B}\rho_B(x_B)dx_B. \tag{A10}$$

This polarization is *multivalued*, and the polarization traditionally used in LGD models corresponds to the polarization difference, namely $\Delta p = p(\delta) - p(\delta = 0)$.

3. Delta functions

Let us confirm that Eq. (A10) gives the correct result in the case of point charges. In this case,

$$\rho_A = \rho_{A0}\delta_f\left(x - \frac{a}{4}\right), \tag{A11}$$

$$\rho_B = \rho_{B0}\delta_f\left(x - \frac{3a}{4} - \delta\right), \tag{A12}$$

where δ_f is the Dirac delta function. Thus,

$$p = e_c\left(\frac{1}{2} - \frac{\delta}{a} + n\right), n \in \mathbb{Z}. \tag{A13}$$

This is exactly the polarization lattice calculated using conventional methods [64]. Choosing the $n = 0$ branch,

$$\Delta p = \left(\frac{e_c}{2} - \frac{e_c\delta}{a}\right) - \frac{e_c}{2} = -\frac{e_c\delta}{a}. \tag{A14}$$

4. PFC polarization

In this case, ρ_i are defined by Eqs. (3), (6), and (7). Then

$$p = \frac{e_c}{2\pi}\mathrm{Im}\ln\frac{A^2\pi^2}{q^2}e^{2\pi i(-\delta/a+1/2)}. \tag{A15}$$

If $A \neq 0$, then

$$\Delta p = -\frac{e_c\delta}{a} \tag{A16}$$

as before. However, if $A = 0$, then the polarization is undefined since the $\ln 0$ is undefined. In a square 2D system, each polarization component is defined the same as in 1D, and

$$p_i = \frac{e_c}{2\pi}\mathrm{Im}\ln\int_V e^{iqx_{i,A}}\rho_A(\boldsymbol{x}_A)d\boldsymbol{x}_A \times \int_V e^{-iqx_{i,B}}\rho_B(\boldsymbol{x}_B)d\boldsymbol{x}_B. \tag{A17}$$

Note that even if ρ_i are general expansions of the form Eq. (13) and (14), the polarization is only a function of the first modes because $q = 2\pi/a = |q_{\{10\}}|$. Algebraically, this is expressed in the integral

$$\int_V e^{-iqx}\rho_B(x,y)dxdy = -A_{10}e^{-iq\delta_x}. \tag{A18}$$

Consequently, Eq. (A17) only depends on the first mode of ρ_i, and

$$\Delta\boldsymbol{p} = -\frac{e_c\boldsymbol{\delta}}{a} \propto -\frac{\boldsymbol{\delta}}{a} \tag{A19}$$

(unless $A_{\{10\}} = 0$, in which case the polarization is undefined).

APPENDIX B: CALCULATING POLARIZATIONS

Displacements were calculated for numerical simulations as follows. First, the maxima of n_A and n_B were calculated by fitting to a quadratic paraboloid, as described in Ref. [67]. These maxima were interpreted as the atomic positions. Then for each B atom, the four nearest A atoms were calculated. The displacement vector was defined to be the vector from the centroid of these four A atoms to B. Note that under this definition, the displacement vector is calculated incorrectly at dislocations. This is the origin of the off-colored regions at the dislocations in Fig. 7. A possible alternative, albeit more complicated, approach for calculating the displacement vector is to equilibrate the entire system in the unpolarized state and then to define the displacement as the offset in the atomic positions compared to the unpolarized reference structure. This approach has the advantage of giving meaningful values at dislocations.

[1] A. Morriss-Andrews and J.-E. Shea, Annu. Rev. Phys. Chem. **66**, 643 (2015).
[2] A. Yamanaka, K. McReynolds, and P. W. Voorhees, Acta Mater. **133**, 160 (2017).
[3] S. O. Nielsen, C. F. Lopez, G. Srinivas, and M. L. Klein, J. Phys.: Condens. Matter **16**, R481 (2004).
[4] W. J. Boettinger, J. A. Warren, C. Beckermann, and A. Karma, Annu. Rev. Mater. Res. **32**, 163 (2002).
[5] A. Chatterjee and D. G. Vlachos, J. Comput,-Aided Mater. Des. **14**, 253 (2007).
[6] A. Laio and F. L. Gervasio, Rep. Prog. Phys. **71**, 126601 (2008).
[7] A. Z. Guo, E. Sevgen, H. Sidky, J. K. Whitmer, J. A. Hubbell, and J. J. de Pablo, J. Chem. Phys. **148**, 134108 (2018).
[8] K. R. Elder and M. Grant, Phys. Rev. E **70**, 051605 (2004).
[9] A. K. Rappe, C. J. Casewit, K. S. Colwell, W. A. Goddard, and W. M. Skiff, J. Am. Chem. Soc. **114**, 10024 (1992).
[10] A. Jaatinen, C. V. Achim, K. R. Elder, and T. Ala-Nissila, Phys. Rev. E **80**, 031602 (2009).
[11] K.-A. Wu, A. Adland, and A. Karma, Phys. Rev. E **81**, 061601 (2010).
[12] N. Pisutha-Arnond, V. W. L. Chan, M. Iyer, V. Gavini, and K. Thornton, Phys. Rev. E **87**, 013313 (2013).
[13] V. Fallah, N. Ofori-Opoku, J. Stolle, N. Provatas, and S. Esmaeili, Acta Mater. **61**, 3653 (2013).
[14] V. Fallah, B. Langelier, N. Ofori-Opoku, B. Raeisinia, N. Provatas, and S. Esmaeili, Acta Mater. **103**, 290 (2016).
[15] P. Hirvonen, M. M. Ervasti, Z. Fan, M. Jalalvand, M. Seymour, S. M. Vaez Allaei, N. Provatas, A. Harju, K. R. Elder, and T. Ala-Nissila, Phys. Rev. B **94**, 035414 (2016).
[16] D. Taha, S. K. Mkhonta, K. R. Elder, and Z.-f. Huang, Phys. Rev. Lett. **118**, 255501 (2017).
[17] M. Greenwood, N. Provatas, and J. Rottler, Phys. Rev. Lett. **105**, 045702 (2010).
[18] M. Greenwood, J. Rottler, and N. Provatas, Phys. Rev. E **83**, 031601 (2011).
[19] K. R. Elder, N. Provatas, J. Berry, P. Stefanovic, and M. Grant, Phys. Rev. B **75**, 064107 (2007).
[20] J. Luce and K. Thornton, APS March Meeting Abstracts (2018), p. V12.007.
[21] V. W. L. Chan, An in-depth examination of a thermodynamic framework for the phase-field crystal model, Ph.D. thesis, University of Michigan, 2015.
[22] Y. Waseda, *The Structure of Non-Crystalline Materials: Liquids and Amorphous Solids* (McGraw-Hill, New York, 1980), pp. 254–291.
[23] E. Alster, K. R. Elder, J. J. Hoyt, and P. W. Voorhees, Phys. Rev. E **95**, 022105 (2017).
[24] E. Alster, D. Montiel, K. Thornton, and P. W. Voorhees, Phys. Rev. Mater. **1**, 060801 (2017).
[25] M. Greenwood, N. Ofori-Opoku, J. Rottler, and N. Provatas, Phys. Rev. B **84**, 064104 (2011).
[26] K. L. M. Elder, M. Seymour, M. Lee, M. Hilke, and N. Provatas, Philos. Trans. R. Soc., A **376**, 20170211 (2018).
[27] Y. Huang, J. Wang, Z. Wang, J. Li, and C. Guo, Phys. Rev. E **95**, 043307 (2017).
[28] W.-J. Yin, J.-H. Yang, J. Kang, Y. Yan, and S.-H. Wei, J. Mater. Chem. A **3**, 8926 (2015).
[29] D. Bi, W. Tress, M. I. Dar, P. Gao, J. Luo, C. Renevier, K. Schenk, A. Abate, F. Giordano, J.-P. Correa Baena, J.-D. Decoppet, S. M. Zakeeruddin, M. K. Nazeeruddin, M. Gra tzel, and A. Hagfeldt, Sci. Adv. **2**, e1501170 (2016).
[30] Z.-K. Tan, R. S. Moghaddam, M. L. Lai, P. Docampo, R. Higler, F. Deschler, M. Price, A. Sadhanala, L. M. Pazos,

D. Credgington, F. Hanusch, T. Bein, H. J. Snaith, and R. H. Friend, Nat. Nanotechnol. **9**, 687 (2014).
[31] M. J. Haun, E. Furman, S. J. Jang, H. A. McKinstry, and L. E. Cross, J. Appl. Phys. **62**, 3331 (1987).
[32] B. A. Strukov and A. P. Levanyuk, *Ferroelectric Phenomena in Crystals* (Springer, Berlin, 1998).
[33] J. Mangeri, Y. Espinal, A. Jokisaari, S. Pamir Alpay, S. Nakhmanson, and O. Heinonen, Nanoscale **9**, 1616 (2017).
[34] S. Liu, I. Grinberg, and A. M. Rappe, Nature **534**, 360 (2016).
[35] J. Hlinka and P. Márton, Phys. Rev. B **74**, 104104 (2006).
[36] P. Marton, I. Rychetsky, and J. Hlinka, Phys. Rev. B **81**, 144125 (2010).
[37] L.-Q. Chen, J. Am. Ceram. Soc. **91**, 1835 (2008).
[38] N. Faghihi, N. Provatas, K. R. Elder, M. Grant, and M. Karttunen, Phys. Rev. E **88**, 032407 (2013).
[39] N. Faghihi, S. Mkhonta, K. R. Elder, and M. Grant, Eur. Phys. J. B **91**, 55 (2018).
[40] M. Seymour, F. Sanches, K. Elder, and N. Provatas, Phys. Rev. B **92**, 184109 (2015).
[41] M. Seymour and N. Provatas, Phys. Rev. B **93**, 035447 (2016).
[42] Z. L. Wang, Z. Liu, and Z. F. Huang, Phys. Rev. B **97**, 180102(R) (2018).
[43] Edited by M. I. Aroyo, *International Tables for Crystallography*, Vol. A (International Union of Crystallography, Chester, England, 2016).
[44] S. Galam, Phys. Rev. B **31**, 1554 (1985).
[45] H. Cohen, in *Number Theory* (Springer, New York, 2007), pp. 1–8.
[46] J. Mellenthin, A. Karma, and M. Plapp, Phys. Rev. B **78**, 184110 (2008).
[47] N. Goldenfeld, B. P. Athreya, and J. A. Dantzig, Phys. Rev. E **72**, 020601(R) (2005).
[48] Y. L. Li, S. Y. Hu, Z. K. Liu, and L. Q. Chen, Appl. Phys. Lett. **78**, 3878 (2001).
[49] H.-L. Hu and L.-Q. Chen, J. Am. Ceram. Soc. **81**, 492 (1998).
[50] D. Vanderbilt and M. H. Cohen, Phys. Rev. B **63**, 094108 (2001).
[51] K. M. Rabe, M. Dawber, C. Lichtensteiger, C. H. Ahn, and J.-M. Triscone, *Physics of Ferroelectrics*, Topics in Applied Physics, Vol. 105 (Springer, Berlin, Heidelberg, 2007), pp. 1–30.
[52] S. Nambu and D. A. Sagala, Phys. Rev. B **50**, 5838 (1994).
[53] W. Cao, Ferroelectrics **375**, 28 (2008).
[54] N. Pisutha-Arnond, V. W. L. Chan, K. R. Elder, and K. Thornton, Phys. Rev. B **87**, 014103 (2013).
[55] Z.-L. Wang, Z.-F. Huang, and Z. Liu, Phys. Rev. B **97**, 144112 (2018).
[56] Y. L. Li, S. Y. Hu, Z. K. Liu, and L. Q. Chen, Appl. Phys. Lett. **81**, 427 (2002).
[57] B. Lee, S. M. Nakhmanson, and O. Heinonen, Appl. Phys. Lett. **104**, 262906 (2014).
[58] Y. L. Li, S. Y. Hu, Z. K. Liu, and L. Q. Chen, Acta Mater. **50**, 395 (2002).
[59] R. K. Behera, C.-W. Lee, D. Lee, A. N. Morozovska, S. B. Sinnott, A. Asthagiri, V. Gopalan, and S. R. Phillpot, J. Phys.: Condens. Matter **23**, 175902 (2011).
[60] B. Meyer and D. Vanderbilt, Phys. Rev. B **65**, 104111 (2002).
[61] E. Holm, D. Srolovitz, and J. Cahn, Acta Metall. Mater. **41**, 1119 (1993).
[62] J. Cahn and E. Van Vleck, Acta Mater. **47**, 4627 (1999).
[63] A. Jain, J. R. Errington, and T. M. Truskett, Soft Matter **9**, 3866 (2013).
[64] N. A. Spaldin, J. Solid State Chem. **195**, 2 (2012).
[65] R. Resta, Phys. Rev. Lett. **80**, 1800 (1998).
[66] R. Resta, Eur. Phys. J. B **91**, 100 (2018).
[67] E. J. Schwalbach, J. A. Warren, K.-A. Wu, and P. W. Voorhees, Phys. Rev. E **88**, 023306 (2013).